Microstructure from ferroelastic transitions using strain pseudospin clock models in two and three dimensions: A local mean-field analysis

Romain Vasseur,[1,2] Turab Lookman,[1] and Subodh R. Shenoy[3]
[1]*Theoretical Division and Center for Nonlinear Studies, Los Alamos National Laboratory, Los Alamos, New Mexico 87545, USA*
[2]*École Normale Supérieure de Lyon, 46 Allée d'Italie, 69007 Lyon, France*
[3]*School of Physics, University of Hyderabad, Hyderabad 500046, India*

(Received 27 June 2010; revised manuscript received 6 September 2010; published 30 September 2010)

We show how microstructure can arise in first-order ferroelastic structural transitions, in two and three spatial dimensions, through a local mean-field approximation of their pseudospin Hamiltonians, that include anisotropic elastic interactions. Such transitions have symmetry-selected physical strains as their N_{OP}-component order parameters, with Landau free energies that have a single zero-strain "austenite" minimum at high temperatures, and spontaneous-strain "martensite" minima of N_V structural variants at low temperatures. The total free energy also has gradient terms, and power-law anisotropic effective interactions, induced by "no-dislocation" St Venant compatibility constraints. In a reduced description, the strains at Landau minima induce temperature dependent, clocklike $\mathbb{Z}_{N_V+1}$ Hamiltonians, with N_{OP}-component strain-pseudospin vectors $\vec{S}$ pointing to N_V+1 discrete values (including zero). We study elastic texturing in five such first-order structural transitions through a local mean-field approximation of their pseudospin Hamiltonians, that include the power-law interactions. As a prototype, we consider the two-variant square/rectangle transition, with a one-component pseudospin taking $N_V+1=3$ values of $S=0,\pm 1$, as in a generalized Blume-Capel model. We then consider transitions with two-component ($N_{OP}=2$) pseudospins: the equilateral to centered rectangle ($N_V=3$); the square to oblique polygon ($N_V=4$); the triangle to oblique ($N_V=6$) transitions; and finally the three-dimensional (3D) cubic to tetragonal transition ($N_V=3$). The local mean-field solutions in two-dimensional and 3D yield oriented domain-wall patterns as from continuous-variable strain dynamics, showing the discrete-variable models capture the essential ferroelastic texturings. Other related Hamiltonians illustrate that structural transitions in materials science can be the source of interesting spin models in statistical mechanics.

DOI: 10.1103/PhysRevB.82.094118 PACS number(s): 81.30.Kf, 64.70.Nd, 05.50.+q, 11.10.Lm

I. INTRODUCTION

Ferroelastic crystals undergo diffusionless structural transitions that are first order, and on cooling show a reduction in symmetry to two or more spontaneously strained states (or "variants") which can be transformed between one another by stress.[1,2] These transitions are often studied through minimizing the Landau free energies[3] in terms of appropriate continuous variables, such as displacements, phase fields, or strains.[4–7] Although homogeneous, single-variant martensite states are the global minimum, elastic heterogeneities or metastable domain-wall patterns are experimentally found,[8] that are locked in to preferred crystallographic directions.[9] This orientation arises through a balance between the Landau energies nonlinear in the order-parameter (OP) strain, the short-range gradient costs, or Ginzburg energies, and the effectively long-range elastic energies[10] or power-law anisotropic interactions, that orient the domain walls.[5,7,10] The power-law interactions result from enforcing St Venant "compatibility" constraints[11,12] between the strain components so that the displacements are continuous, with no dislocations generated on cooling. Continuous-variable models have been used to study microstructures under various conditions, including strain-rate dependence;[13] and the effects of finite size on martensitic growth in an austenitic matrix.[14]

Models in terms of *discrete* structure variables or "pseudospins" have also been used to study these ferroelastic transitions.[15,16] (Similar in spirit to discrete strains, analytic "minimizing sequences" consider tentlike displacement profiles or flat strain variants, on either sides of domain walls.[2]) Recently, model pseudospin Hamiltonians induced by the scaled free energies for several specific transitions in two-dimensional (2D) and three-dimensional (3D) have been proposed.[17] The model Hamiltonian is simply the total scaled[18] free energy evaluated at the Landau minima in the OPs. The pseudospins are "arrows" in N_{OP}-dimensional order-parameter space, pointing to the N_V variant minima, and to the zero-strain turning point. The Hamiltonian includes a temperature-dependent on-site term quadratic in the pseudospins from the Landau term, a nearest-neighbor ferromagnetic interaction between pseudospins from the Ginzburg term, and a pseudospin power-law interaction from the St Venant term. The pseudospin models are like $\mathbb{Z}_{N_V+1}$ clock models[19] generalized to include a spin-zero state and may be termed "clock-zero" models.[17] A three-state spin-1 type model for the transition of square to rectangle unit cells (with $N_{OP}=1$, $N_V=2$) has found glasslike behavior on slow cooling using a local mean-field approximation.[17]

In this work we consider pseudospin models in the *local mean-field approximation* under temperature quenches, for five structural transitions: four in two spatial dimensions[20] and one in three spatial dimensions.[7] Apart from the single order parameter ($N_{OP}=1$) square/rectangle case that is first studied as a simple prototype, the other four transitions all have two-component ($N_{OP}=2$) pseudospins. The transitions are (i) the square to rectangle (2D version of the tetragonal/

orthorhombic transition such as in Yittrium Barium Oxide (YBCO); (ii) the square to oblique polygon; (iii) the triangle to centered rectangle (2D version of hexagonal to orthorhombic transition such as in lead orthovanadate[4,6,7]); (iv) the triangle to oblique; and (v) in 3D, the cubic to tetragonal (CT) transition (as in FePd). For these five transitions, the (nonzero) pseudospin arrows point, respectively,[17] to the two ends of a line, and to the corners of a square, a triangle, a hexagon, and a triangle, with the number of pseudospin variant states thus being, respectively, $N_V=2$, 4, 3, 6, and 3. We show that these discrete-variable models, despite their simplicity, produce local-mean-field microstructure in one- and two-component strain pseudospins in agreement with continuous-variable strain simulations,[4–7] that can be computationally more intensive. We thus find parallel twins for the square/rectangle and cubic/tetragonal transitions; nested stars for the equilateral/isosceles triangle transition; and tilted oblique domains for the square/oblique, and triangle/oblique transitions.

The generalized clock model of strain pseudospins is a statistical mechanics description of the ferroelastic transitions in materials science. It conceptually links long lived, metastable martensitic twins (even without quenched disorder) to Potts-model and clock-model descriptions of glasses,[19] and may be relevant to recent quenched-disorder strain glass behavior in martensitic alloys.[21]

The plan of the paper is as follows. In Sec. II we outline the derivation[17] of the pseudospin Hamiltonians, and of compatibility potentials for the four 2D transitions. Our mean-field microstructure results are in Sec. III where we first consider the two-variant square/rectangle case as a prototype, its response to external stress, and its relation to the spin-1 Blume-Capel model.[21] We then consider local mean-field microstructure for the three-variant triangle to centered-rectangle transition; the four-variant square/oblique transition; and the six-variant triangle/oblique transition. Turning to 3D, Sec. IV considers the local mean-field microstructure for the three-variant cubic/tetragonal transition with its compatibility potential stated in the Appendix. In Sec. V we mention other related spin models of interest in statistical mechanics. The final Sec. VI has a summary and conclusion.

II. PSEUDOSPIN HAMILTONIANS IN TWO SPATIAL DIMENSIONS

The free-energy functionals describing ferroelastic structural transitions can be written in terms of the *physical* strains that are symmetry-specific linear combinations of the Cartesian strain-tensor components. The Landau terms are invariant polynomials of the $N_{\rm OP}$ order-parameter strains and have N_V minima. The free energies have many material-dependent elastic coefficients that are not always known, or are fitted to experiment only for specific materials. However, the spontaneous order-parameter strain magnitude at the first-order transition temperature is a small parameter. Following Barsch and Krumhansl[18] a scaling procedure has been applied[17] to four 3D transitions and five 2D transitions to obtain scaled Landau free energies that (to leading order in the small parameter) show universality at their minima, where any internal elastic constants are scaled out, and material dependence is only in an overall elastic-energy prefactor. "Geometric nonlinearities" are higher order in the spontaneous strain and are neglected, as a perturbative first approximation. Then different materials with the same transition, fall into the same "quasiuniversality" class, with common behavior at the scaled minima, that lie at the corners and centers of the same "polyhedron" in $N_{\rm OP}$-dimensional order-parameter space. This is useful in strain-variable dynamics. It also immediately suggests a reduced description of ferroelastics, in terms of discrete-strain statistical variables or vector "pseudospins," directed to these minima.

A specific reduction procedure was proposed[17] to obtain pseudospin Hamiltonians by evaluating *scaled* free energies evaluated at their Landau minima. The basic idea is quite simple. (i) Scale the total free energy to dimensionless form, including the specifically calculated compatibility-induced power-law interaction term, and the gradient term. Write the Landau free energy in polar coordinates in OP space, with the austenite minimum at the origin, and N_V martensite minima located on a circle in N_V discrete angular directions. (ii) Set the radial OP magnitude to its common temperature-dependent Landau-minimum value, and replace the OP-minima directional angles by discrete vectors pointing to these N_V+1 minima on the circle, and at the center. (iii) The total free energy evaluated at minima is then the model Hamiltonian for the vector pseudospins, that have $N_{\rm OP}$ spin components, and N_V+1 values. The remaining model coefficients are then not just arbitrary, but are related through the parent free energy, to the scaled temperature, to the scaled energy cost of an elastic domain-wall segment, and to the scaled bulk stiffness.

We outline below the derivation[17] of the pseudospin Hamiltonians and compatibility potentials in two spatial dimensions, for the square/rectangle, triangle/centered-rectangle, square/oblique, and triangle/oblique transitions, with number of variants $N_V=2$, 3, 4, and 6, respectively. The 3D case is considered later.

A. Square to rectangle (SR) Hamiltonian: $N_{\rm OP}=1$, $N_V=2$

Consider the prototypical square-to-rectangle or "SR" transition that is a two-dimensional analog of a tetragonal to orthorhombic transition. For small distortions, the components of the symmetric Cartesian strain tensor are given by $e_{\mu\nu}=1/2(\partial_\mu u_\nu+\partial_\nu u_\mu)$, where $\vec{u}(\vec{r})$ is the displacement vector and $\mu,\nu=x,y$. We define linear combinations of the Cartesian components as three physical strains, describing compressional (e_1), deviatoric (e_2), and shear (e_3) distortions,

$$e_1=\frac{c_1}{2}(e_{xx}+e_{yy}),\quad e_2=\frac{c_2}{2}(e_{xx}-e_{yy}),\quad e_3=\frac{c_3}{2}(e_{xy}+e_{yx}), \tag{1}$$

where c_1, c_2, and c_3 are symmetry-specific constants.[7] For the square reference lattice, $c_1=c_2=\sqrt{2}$ and $c_3=1$. For the equilateral triangle reference lattice $c_1=c_2=c_3=1$. The pseudospin Hamiltonian is obtained by the three steps given above, that we follow for all transitions.

1. Scaled free energy and compatibility potential

For the SR case, the deviatoric strain e_2 is the OP. The compressional and shear strains are the non-OP strains. The scaled free energy is $F=E_0\bar{F}$, where the overall E_0 is an elastic energy per unit cell and the dimensionless $\bar{F}=\bar{F}_L+\bar{F}_G+\bar{F}_{non}$ is a sum of three terms,

$$\bar{F}_L=\sum_{\vec{r}}\bar{f}_L(e_2),\quad \bar{F}_G=\sum_{\vec{r}}\bar{f}_G(\vec{\nabla}e_2),\quad \bar{F}_{non}=\sum_{\vec{r}}\bar{f}_{non}(e_1,e_3). \tag{2}$$

where $\Sigma_{\vec{r}}\to\int d^2r/a_0^2$ runs over all positions and a_0 is a lattice scale for a computational grid.

The dimensionless, scaled Landau free-energy density in coordinate space is sixth order in $e_2(\vec{r})$ to give a first-order transition,[5,7]

$$\bar{f}_L(e_2)=(\tau-1)e_2^2+e_2^2(e_2^2-1)^2. \tag{3}$$

A scaled temperature is defined by

$$\tau\equiv(T-T_c)/(T_0-T_c). \tag{4}$$

There can be three $\partial f_L/\partial e_2=0$ minima: at zero-strain $e_2=0$ austenite and at two martensite variant minima of nonzero strain, $e_2=\pm\bar{\varepsilon}(\tau)$. The order-parameter magnitude $\bar{\varepsilon}$ at the variant minima is

$$\bar{\varepsilon}(\tau)=\left[\frac{2}{3}(1+\sqrt{1-3\tau/4})\right]^{1/2}. \tag{5}$$

On cooling below the upper spinodal $\tau=4/3$, two martensite variants appear; they become degenerate with the austenite zero state at $\tau=1$ or $T=T_0$ when $\bar{\varepsilon}(\tau=1)=1$; and for $\tau<1$ the martensite wells become lower in energy. The austenite minimum disappears below the lower spinodal $\tau=0$ or $T=T_c$.

The cost of creating interfaces or domain walls is given by the usual Ginzburg term with ξ a wall thickness scale,

$$\bar{F}_G=\sum_{\vec{r}}\xi^2[\vec{\nabla}e_2(\vec{r})]^2=\sum_{\vec{k}}\xi^2\vec{k}^2|e_2(\vec{k})|^2. \tag{6}$$

Finally, the non-OP strain energy is simply harmonic in compressional (e_1) and shear (e_3) strains,

$$\bar{F}_{non}=\sum_{\vec{r},i=1,3}\frac{1}{2}A_ie_i(\vec{r})^2=\sum_{\vec{k},i=1,3}\frac{1}{2}A_i|e_i(\vec{k})|^2. \tag{7}$$

The scaled compressional and shear elastic constants can be expressed in terms of the (unscaled) elastic constants C_{ij} in the Voigt notation, evaluated at T_0. For the cubic case,[17] $A_1=(C_{11}+2C_{12})/(C_{11}-C_{12})$. The ratio A_1/A_3 is taken as fixed in simulations, for simplicity.

For $\vec{k}=0$ uniform contributions, the optimum non-OP strains are zero, at the parabolic $f_{non}=0$ minimum. For spatially varying $\vec{k}\neq0$ contributions, the non-OP strains are to be minimized subject to the St Venant compatibility constraint[5,7,11,12] that says distorted unit cells fit together in a smoothly compatible fashion, without defectslike dislocations, so the displacement field is single valued. The St. Venant conditions in the Cartesian strain tensor $\mathbf{e}$ are[11,12] (with "T" a transpose),

$$\vec{\nabla}\times(\vec{\nabla}\times\mathbf{e})^{\mathrm{T}}=0. \tag{8}$$

In two dimensions, the constraint in terms of physical strains of Eq. (1) is

$$\frac{1}{c_1}\vec{\nabla}^2e_1-\frac{1}{c_2}(\partial_x^2-\partial_y^2)e_2-\frac{2}{c_3}\partial_x\partial_ye_3=0 \tag{9}$$

or in Fourier space

$$O_1e_1(\vec{k})+O_2e_2(\vec{k})+O_3e_3(\vec{k})=0, \tag{10}$$

where the compatibility coefficients are

$$O_1=\frac{-\vec{k}^2}{c_1},\quad O_2=\frac{k_x^2-k_y^2}{c_2},\quad O_3=\frac{2k_xk_y}{c_3}. \tag{11}$$

The constrained minimization can be done through Lagrange multipliers[5] or by a direct substitution of the constrained solution[17] $e_1=-(O_2e_2+O_3e_3)/O_1$ of Eq. (10), into the non-OP free energy of Eq. (7),

$$\bar{f}_{non}=\sum_{\vec{k}\neq0}\frac{1}{2}[A_1|(O_2e_2+O_3e_3)/O_1|^2+A_3|e_3|^2]. \tag{12}$$

A free minimization in the remaining non-OP strain e_3 determines it in terms of the OP e_2. In fact, $e_i=-(O_iO_2/A_i)/[(O_1^2/A_1)+(O_3^2/A_3)]$ for $i=1,3$. Substituting into Eq. (7) yields the compatibility-induced interaction $\bar{F}_{compat}(e_2)\equiv\bar{F}_{non}(e_1,e_3)$, where

$$\bar{F}_{compat}=\sum_{\vec{k}}\frac{A_1}{2}U(\vec{k})|e_2(\vec{k})|^2. \tag{13}$$

The compatibility kernel U in Fourier space is

$$A_1U(\vec{k})=\nu(\vec{k})\frac{O_2^2}{[(O_1^2/A_1)+(O_3^2/A_3)]} \tag{14}$$

or explicitly from Eq. (11), and $c_1=c_2=\sqrt{2}$, $c_3=1$,

$$U(\vec{k})=\nu(\vec{k})\frac{(k_x^2-k_y^2)^2}{k^4+8\dfrac{A_1}{A_3}k_x^2k_y^2}. \tag{15}$$

Here the prefactor $\nu(\vec{k})\equiv1-\delta_{\vec{k},0}$ is inserted to make $f_{non}\sim U$ vanish for $\vec{k}=0$ uniform non-OP strains, as mentioned. In coordinate space, this is a power-law interaction between OP strains $U(\vec{R})\sim1/R^d$, with sign variation in angular directions yielding zero angular average $[\Sigma_{\vec{R}}U(\vec{R})\sim U(\vec{k}=0)=0]$, so it is not "long range" in the isotropic Coulomb $\sim1/R^{d-2}$ sense. The angular part varies as $-(1-\eta\cos4\theta)/(\eta-\cos4\theta)^2$ where η depends on moduli A_1, A_3. This corrects expression 3.41c in Ref. 7(a). The power-law anisotropic interactions are easily evaluated in Fourier space, and one need not resort to uncontrolled coordinate-space truncations to near-neighbor couplings, that may leave out some essential physics of the transition. In coordinate space,

$$\bar{F}_{compat}(e_2)=\frac{1}{2}\sum_{\vec{r},\vec{r}'}A_1U(\vec{r}-\vec{r}')e_2(\vec{r})e_2(\vec{r}'). \tag{16}$$

The formal partition function

$$Z = \int \prod_{\vec{r}} de_2(\vec{r}) \exp(-\beta F[e_2(\vec{r})]), \tag{17}$$

is dominated by free-energy textural minima, that may be asymptotically found in a time dependent Ginzburg Landau (TDGL) or relaxational dynamics, as done elsewhere,[7]

$$\frac{\partial e_2(\vec{r},t)}{\partial t} = -\frac{\delta F}{\delta e_2(\vec{r},t)}. \tag{18}$$

2. Continuous strains to discrete pseudospins

One can approximate the partition function by retaining only the Landau minima at fixed OP-magnitude values $|e_2| = \bar{\varepsilon}(\tau)$, and different OP signs (or in general, different angular directions of minima), while neglecting fluctuations about these minima. The continuous-variable strains are then replaced by discrete-variable pseudospins[17]

$$e_2(\vec{r}) \to \bar{\varepsilon}(\tau) S(\vec{r}), \tag{19}$$

where the pseudospin has the three values $S(\vec{r}) = 0, \pm 1$, to locate the minima at $e_2 = 0, \pm \bar{\varepsilon}(\tau)$. Although in zero stress the uniform austenite state is no longer a Landau minimum below the lower spinodal $\tau = 0$, the surrounding nonuniform textures can exert local internal stresses to locally favor the zero value, even at low temperatures. Also, the free energy in OP strain always has a turning point at the origin to support dynamical transient zeros, that although few in number, could play a catalytic role in microstructural evolution.[17] Hence we retain zero spin values at all temperatures, allowing their permanent/transient existence to be determined dynamically.

With this substitution and $S^6 = S^4 = S^2 = 1, 0$, the approximated Landau free-energy density at the minima can be written as[17]

$$\bar{f}_L = \bar{\varepsilon}^2(\tau) g_L(\tau) S^2(\vec{r}), \quad g_L \equiv (\tau - 1) + (\bar{\varepsilon}^2 - 1)^2, \tag{20}$$

where $\bar{\varepsilon}$ is in Eq. (5).

3. Reduced pseudospin Hamiltonian

The partition function of Eq. (17) reduces to a sum over all the pseudospin configurations, with a temperature-dependent effective Hamiltonian in the Boltzmann weight, that can then be studied by the usual methods of statistical mechanics. Substituting Eq. (19) into the total scaled free energy directly yields the Hamiltonian in coordinate space,

$$H(S) \equiv \bar{F}(e_2 \to \bar{\varepsilon} S), \tag{21}$$

where

$$\beta H(S) = \frac{D_0}{2} \left[\sum_{\vec{r}} \{ g_L S^2(\vec{r}) + \xi^2 (\vec{\nabla} S)^2 \} + \sum_{\vec{r},\vec{r}'} \frac{A_1}{2} U(\vec{r} - \vec{r}') S(\vec{r}) S(\vec{r}') \right] \tag{22}$$

and $D_0 \equiv 2E_0 \bar{\varepsilon}(\tau)^2 / T$. This has the form of a generalized spin-1 Blume-Capel model[22] as discussed later but with temperature-dependent coefficients and power-law interactions. The Hamiltonian is diagonal in Fourier space,[17]

$$\beta H = \frac{1}{2} \sum_{\vec{k}} Q_0(\vec{k}) |S(\vec{k})|^2, \tag{23}$$

where

$$Q_0(\vec{k}) \equiv D_0 \left[g_L(\tau) + \xi^2 \vec{k}^2 + \frac{A_1}{2} U(\vec{k}) \right]. \tag{24}$$

B. Triangle/centered rectangle (TCR) Hamiltonian: $N_{OP}=2$, $N_V=3$

Consider a two-dimensional crystal with equilateral triangles transforming to isosceles triangles, with three possible such variants ($N_V = 3$), as there are three sides that can become the unequal side. The unit cell changes from an equilateral triangle to a centered rectangle. This "TCR" transition is the 2D version of the hexagonal to orthorhombic transition observed in lead orthovanadate.[8] There are two order parameters:[4,7,17,20] the deviatoric strain e_2 and the shear strain e_3. The single non-OP variable is the bulk dilatation or compressional strain e_1. Just like this TCR case, the square/oblique, triangle/oblique, and cubic/tetragonal transitions also have the same OP (e_2, e_3) and a single non-OP strain e_1, but of course are distinguished by their different, transition-specific Landau polynomials, that induce different N_V directions of the vector pseudospins.

1. Scaled free energy and compatibility potential

The free-energy functional, invariant under the triangular point-group symmetry, is

$$\bar{F} = \sum_{\vec{r}} \{ \bar{f}_L(e_2, e_3) + \bar{f}_G(\vec{\nabla} e_2, \vec{\nabla} e_3) + \bar{f}_{non}(e_1) \}. \tag{25}$$

The Landau free energy f_L for the TCR case describes the first-order phase transition between the single high-symmetry austenite phase and the $N_V = 3$ martensite variants. It has a third-order term invariant under equilateral triangle symmetries, $I_3 \equiv e_2^3 - 3e_2 e_3^2$. In scaled form, in coordinate space

$$\bar{f}_L(e_2, e_3) = \tau(e_2^2 + e_3^2) - 2(e_2^3 - 3e_2 e_3^2) + (e_2^2 + e_3^2)^2. \tag{26}$$

Figure 1 shows the Landau free energy with three variant minima, for a low temperature.

In polar coordinates in OP space, the order-parameter vector is $\vec{e}(\vec{r}) = (e_2, e_3) = \varepsilon(\cos\phi, \sin\phi)$ with magnitude $\varepsilon(\vec{r}) \equiv (e_2^2 + e_3^2)^{1/2}$. The Landau free energy in polar coordinates with $\eta_3 \equiv \cos 3\phi$ is[17]

$$\bar{f}_L(\varepsilon, \phi) = [(\tau - 1)\varepsilon^2 + \varepsilon^2(\varepsilon - 1)^2] + 2(1 - \eta_3)\varepsilon^3. \tag{27}$$

The angular dependence is $\bar{f}_L \sim -\cos 3\phi$. The minimum conditions $\partial f_L / \partial \varepsilon = 0$, $\partial f_L / \partial \phi = 0$ yield four minima: at the $\vec{e} = 0$ austenite, and the three variant minima with $\sin 3\phi = 0$, where $\phi = \phi_m = 0, \pi/3, 2\pi/3$, so the last term in Eq. (27) van-

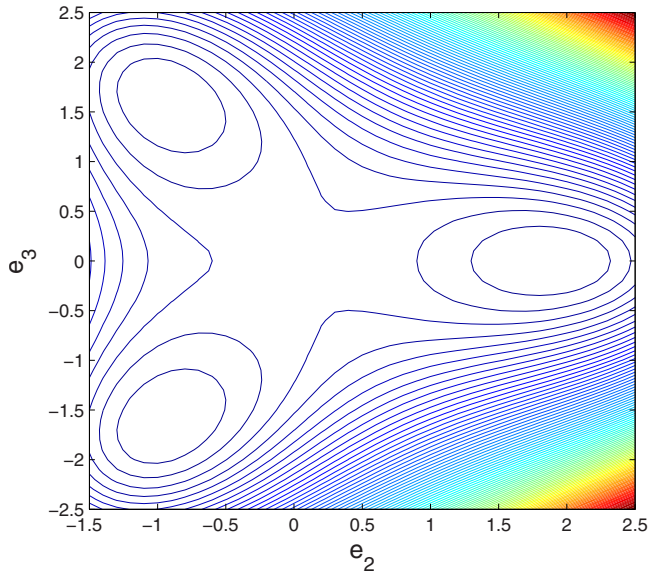

FIG. 1. (Color online) Contour plot in (e_2,e_3) space of the Landau free energy for the TCR transition with parameters $\tau=-2.5$ and $E_0=1$. The three degenerate energy minima correspond to the three martensite variants at this low temperature.

ishes. The three variant minima in the (e_2,e_3) plane form a triangle lying on a circle of radius $\varepsilon=\bar{\varepsilon}(\tau)$, where

$$\bar{\varepsilon}(\tau)=\frac{3}{4}(1+\sqrt{1-8\tau/9}). \tag{28}$$

On cooling below the upper spinodal $\tau=4/3$, two martensite variants appear; they become degenerate with the austenite zero state at $\tau=1$ or $T=T_0$ when $\bar{\varepsilon}(\tau=1)=1$; and for $\tau<1$ the martensite wells become lower in energy. The austenite minimum disappears below the lower spinodal $\tau=0$ or $T=T_c$.

The Ginzburg term $\bar{f}_G$ is quadratic in the OP-strain gradient so

$$\bar{F}_G=\sum_{\vec{r},\ell=2,3}\xi^2(\vec{\nabla}e_\ell)^2=\sum_{\vec{k},\ell=2,3}\xi^2\vec{k}^2|e_\ell(\vec{k})|^2. \tag{29}$$

Finally, the non-OP term is simply harmonic in the single non-OP compressional strain,

$$\bar{F}_{non}(e_1)=\frac{A_1}{2}\sum_{\vec{r}}e_1^2(\vec{r})=\frac{A_1}{2}\sum_{\vec{k}}|e_1(\vec{k})|^2. \tag{30}$$

Substitution of the compatibility solution $e_1(\vec{k})=-(O_2e_2+O_3e_3)/O_1$ as for Eq. (12) immediately yields the St Venant term $\bar{F}_{compat}(e_2,e_3)\equiv\bar{F}_{non}(e_1)$ in terms of the OP,

$$\bar{F}_{compat}=\sum_{\vec{k},\ell,\ell'=2,3}\frac{A_1}{2}U_{\ell\ell'}(\vec{k})e_\ell(\vec{k})e_{\ell'}(\vec{k})^*. \tag{31}$$

The compatibility potential kernel is[7,15]

$$U_{\ell\ell'}=\nu(\vec{k})O_\ell O_{\ell'}/O_1^2 \tag{32}$$

or explicitly from Eq. (11) with $c_1=c_2=c_3=1$,

$$U_{22}=\nu\frac{(k_x^2-k_y^2)^2}{k^2},\quad U_{22}=\nu\frac{(2k_xk_y)^2}{k^2},$$

$$U_{23}=\nu\frac{2k_xk_y(k_x^2-k_y^2)}{k^2}=U_{32}. \tag{33}$$

In coordinate space,

$$\bar{F}_{compat}(e_2,e_3)=\frac{A_1}{2}\sum_{\vec{r},\vec{r}'}\sum_{\ell,\ell'=2,3}U_{\ell\ell'}(\vec{r}-\vec{r}')e_\ell(\vec{r})e_{\ell'}(\vec{r}'), \tag{34}$$

and as before, the power-law potentials fall off in 2D as $U_{\ell\ell'}\sim 1/R^2$.

2. Continuous strains to discrete pseudospins

For the TCR case (and other two-component OP cases), $N_V\geq 3$, but we *do not* simply get a generalized spin-j model with $2j+1$ states on a line, and $j=N_V/2$. Instead we obtain *clocklike* models[17,19] with discrete $\vec{S}$ vector variables pointing to the polyhedron N_V corners and center in $N_{\rm OP}$-dimensional space. Since the zero state is included, these may be termed "clock-zero" $\mathbb{Z}_{N_V+1}$ models.[17] Note that, unlike pure clock $\mathbb{Z}_N$ models,[17] the squared spin $\vec{S}(\vec{r})^2=1,0$ is still a statistical variable and not a constant, because of the zero states.

The continuous-variable strains at minima are replaced by discrete-valued pseudospins,[17]

$$\vec{e}(\vec{r})=\begin{pmatrix}e_2\\e_3\end{pmatrix}\rightarrow\bar{\varepsilon}(\tau)\begin{pmatrix}S_2(\vec{r})\\S_3(\vec{r})\end{pmatrix}, \tag{35}$$

where the two components of the pseudospin have three variant values as in Fig. 1 plus zero,

$$\vec{S}=\begin{pmatrix}0\\0\end{pmatrix},\begin{pmatrix}1\\0\end{pmatrix},\begin{pmatrix}-\frac{1}{2}\\ \pm\frac{\sqrt{3}}{2}\end{pmatrix}. \tag{36}$$

For the $N_V=3$ variants, $\vec{S}=(\cos\phi_m,\sin\phi_m)$ and $\vec{S}^2=1$, with $\phi_m=2\pi(m-1)/3$ and $m=1,2,3$.

With this substitution and $\vec{S}^6=\vec{S}^4=\vec{S}^2=0,1$, the Landau polynomials again collapse into a simple form, bilinear in the pseudospins,

$$\bar{f}_L(\tau)=\bar{\varepsilon}^2g_L\vec{S}^2,\quad g_L(\tau)\equiv\tau-1+(\bar{\varepsilon}-1)^2 \tag{37}$$

with $\bar{\varepsilon}$ as in Eq. (28).

3. Reduced pseudospin Hamiltonian

In coordinate space the total pseudospin Hamiltonian is

$$\beta H = \frac{D_0}{2}\Bigg[\sum_{\vec{r}}\sum_{\ell=2,3}\{g_L S_\ell(\vec{r})^2 + \xi^2|\vec{\nabla}S_\ell(\vec{r})|^2\} + \frac{A_1}{2}\sum_{\vec{r},\vec{r}'}\sum_{\ell,\ell'=2,3} U_{\ell\ell'}(\vec{r}-\vec{r}')S_\ell(\vec{r})S_{\ell'}(\vec{r}')\Bigg] \quad (38)$$

and is a clock-zero $\mathbb{Z}_{3+1}$ model,[17] with $\vec{S}$ having $3+1$ values of Eq. (36), and with a compatibility kernel of Eq. (33). It is again diagonal in Fourier space,

$$\beta H = \frac{1}{2}\sum_{\vec{k}}\sum_{\ell,\ell'} Q_{0,\ell\ell'}(\vec{k})S_\ell(\vec{k})S_{\ell'}(\vec{k})^* \quad (39)$$

with $\vec{S}(\vec{k})^* = \vec{S}(-\vec{k})$, as $\vec{S}(\vec{r})$ is real. Here

$$Q_{0,\ell\ell'}(\vec{k}) \equiv D_0\left[\{g_L(\tau) + \xi^2\vec{k}^2\}\delta_{\ell,\ell'} + \frac{A_1}{2}U_{\ell\ell'}(\vec{k})\right]. \quad (40)$$

C. Square/oblique (SO) Hamiltonian: $N_{OP}=2$, $N_V=4$

We consider the square/oblique or "SO" transition where the transition is driven independently by the deviatoric e_2 and shear e_3 order-parameter strains,[7,17,20] as modified by a sufficiently strong-coupling term.

1. Scaled free energy and compatibility potential

The Landau term has the scaled form

$$\bar{f}_L = \tau(e_2^2+e_3^2) - (4 - C_4'/2)(e_2^4+e_3^4) + 4(e_2^6+e_3^6) - C_4' e_2^2 e_3^2, \quad (41)$$

where C_4' is a material-dependent elastic constant. In polar coordinates, with $\vec{e}=(e_2,e_3)=\varepsilon(\cos\phi,\sin\phi)$, it is[17]

$$\bar{f}_L = [(\tau-1)\varepsilon^2 + \varepsilon^2(\varepsilon^2-1)^2] + \varepsilon^4(3\varepsilon^2 - 2 + C_4'/2)\cos^2 2\phi. \quad (42)$$

The angular dependence is $\bar{f}_L \sim \cos 4\phi$. The five minima from $\partial\bar{f}_L/\partial\varepsilon=0$, $\partial\bar{f}_L/\partial\phi=0$ are the austenite zero state and four variant minima with $\sin 4\phi=0$ in angular directions $\phi=\phi_m=\pi(2m-1)/4$ with $m=1,2,3,4$. The last term in Eq. (42) vanishes at minima, suppressing the C_4' material dependence. The four variant minima in the e_2,e_3 plane for $\tau<4/3$ form a square lying on a circle of radius $\varepsilon=\bar{\varepsilon}(\tau)$, where $\bar{\varepsilon}$ is as in the SR case of Eq. (5).

2. Continuous strains and discrete pseudospins

The strains at minima are replaced by pseudospins as in Eq. (35). The discrete pseudospin has the five values[17]

$$\vec{S} = \begin{pmatrix}0\\0\end{pmatrix}, \begin{pmatrix}1\\0\end{pmatrix}, \begin{pmatrix}\pm\frac{1}{\sqrt{2}}\\ \pm\frac{1}{\sqrt{2}}\end{pmatrix}. \quad (43)$$

For the $N_V=4$ variant minima with $\vec{S}=(\cos\phi_m,\sin\phi_m)$, and $\phi=\phi_m=\pi(2m-1)/4$, where $m=1,2,3,4$, the spin magnitude is unity $\vec{S}^2=1$.

The Landau term becomes

$$\bar{f}_L = \bar{\varepsilon}^2 g_L \vec{S}^2, \quad g_L \equiv \tau - 1 + (\bar{\varepsilon}^2-1)^2 \quad (44)$$

with $\bar{\varepsilon}$ of Eq. (5).

3. Reduced pseudospin Hamiltonian

The Ginzburg and St Venant terms are the same as in the TCR case. The SO case clock-zero Hamiltonian $\mathbb{Z}_{4+1}$ is formally the same as Eq. (38), with $\vec{S}$ having $4+1$ spin directions of Eq. (43), and the same TCR compatibility kernel of Eq. (33).

D. Triangle/oblique (TO) Hamiltonian: $N_{OP}=2$, $N_V=6$

The transition is, as in the TCR case, driven by a two-component OP (Refs. 7, 17, and 20) $\vec{e}\equiv(e_2,e_3)$. Here $N_V=6$, so we need a square of the cubic term, I_3^2 to give six preferred angles.

1. Scaled free energy and compatibility potential

The scaled Landau free energy with up to sixth-order invariants is[17]

$$\bar{f}_L = (\tau-1)I_2 + I_2(I_2-1)^2 + C_6(I_2^3 - I_3^2), \quad (45)$$

where $I_2=\vec{e}^2\equiv\varepsilon^2$, $I_3=e_2^3-3e_2e_3^2$, and C_6 is a material constant.

In polar coordinates with $\eta_3=\cos 3\phi$, this is[17]

$$\bar{f}_L = [(\tau-1)\varepsilon^2 + \varepsilon^2(\varepsilon^2-1)^2] + C_6\varepsilon^6(1-\eta_3^2). \quad (46)$$

The angular dependence is $\bar{f}_L \sim -\cos 6\phi$. Minimizing yields six martensite variants with $\sin 6\phi=0$, at angles $\phi=\phi_m\equiv 2\pi(m-1)/6$, where $m=1,2,\ldots,6$, where the last term in Eq. (46) vanishes, suppressing the C_6 material dependence. The six variants for $\tau<4/3$ form a hexagon in the e_2,e_3 plane, lying on a circle with radius $\varepsilon=\bar{\varepsilon}(\tau)$ of Eq. (5).

2. Continuous strains to discrete pseudospins

With the usual approximation, Eq. (35), of $\vec{e}(\vec{r}) \to \varepsilon(\tau)\vec{S}(\vec{r})$, the pseudospin $\vec{S}(\vec{r})$ has seven values

$$\vec{S} = \begin{pmatrix}0\\0\end{pmatrix}, \begin{pmatrix}\pm 1\\0\end{pmatrix}, \begin{pmatrix}\pm\frac{1}{2}\\ \pm\frac{\sqrt{3}}{2}\end{pmatrix}. \quad (47)$$

The Landau term becomes

$$\bar{f}_L(\tau) = \bar{\varepsilon}(\tau)^2 g_L \vec{S}(\vec{r})^2, \quad g_L(\tau) \equiv (\tau-1) + (\bar{\varepsilon}^2-1)^2 \quad (48)$$

with $\bar{\varepsilon}$ of Eq. (5).

3. Reduced pseudospin Hamiltonian

The Ginzburg and St Venant terms are as in the TR case. The TO case clock-zero $\mathbb{Z}_{6+1}$ Hamiltonian is as in Eq. (38) with $\vec{S}$ having $6+1$ spin values, Eq. (47), and with the compatibility kernel of Eq. (33).

III. LOCAL MEAN FIELD IN TWO SPATIAL DIMENSIONS

With the pseudospin Hamiltonians for SR, TCR, SO, and TO transitions in hand, we now do local mean-field approximations[17] for each of these cases.

A. Square/rectangle mean field: $N_{OP}=1$, $N_V=2$

We write $S(\vec{r})=\sigma(\vec{r})+\delta S(\vec{r})$, where $\sigma(\vec{r})=\langle S(\vec{r})\rangle$ is the spin statistical average and substitute into Hamiltonian (38). Retaining only first-order terms in $\delta S(\vec{r})\equiv S(\vec{r})-\sigma(\vec{r})$, the mean-field Hamiltonian is $H=H_{MF}+\mathcal{O}(\delta S^2)$. A similar approximation, with identical final results, can be done in Fourier space, with $S(\vec{k})=\sigma(\vec{k})+\delta S(\vec{k})$ substituted in Eq. (39).

The mean-field Hamiltonian is then a sum of a local contribution and a constant,

$$\beta H_{MF} \equiv \sum_{\vec{r}} \beta h_{MF}(\vec{r}) - C, \tag{49}$$

where

$$\sum_{\vec{r}} \beta h_{MF}(\vec{r}) \equiv \sum_{\vec{r}} V(\vec{r})S(\vec{r}) = \sum_{\vec{k}} V(\vec{k})S(\vec{k})^* \tag{50}$$

and $C\equiv\frac{1}{2}\langle\Sigma\beta h_{MF}\rangle=\frac{1}{2}\Sigma_{\vec{k}}V(\vec{k})\sigma(\vec{k})^*=\frac{1}{2}\Sigma_{\vec{k}}Q_0|\sigma(\vec{k})|^2$. Here, V in Fourier and coordinate space is

$$\frac{V(\vec{k})}{D_0} = \left[g_L(\tau) + \xi^2 k^2 + \frac{A_1}{2} U(\vec{k}) \right] \sigma(\vec{k}) \tag{51}$$

and

$$\frac{V(\vec{r})}{D_0} = g_L(\tau)\sigma(\vec{r}) - \xi^2 \vec{\nabla}^2 \sigma(\vec{r}) + \frac{A_1}{2} \sum_{\vec{r}'} U(\vec{r}-\vec{r}')\sigma(\vec{r}'). \tag{52}$$

The mean-field partition function is a product of local contributions

$$Z_{MF} = \sum_{\{S\}} e^{-\beta H_{MF}} = \prod_{\vec{r}} \sum_{S(\vec{r})} e^{-\beta h_{MF}(\vec{r})+C}. \tag{53}$$

The self-consistency equation for the statistical average $\sigma(\vec{r})$, with the constant C dropping out, is

$$\sigma(\vec{r}) = \sum_{S(\vec{r})=0,\pm 1} S(\vec{r}) e^{-\beta V(\vec{r})S(\vec{r})} / \sum_{S(\vec{r})=0,\pm 1} e^{-\beta V(\vec{r})S(\vec{r})}, \tag{54}$$

that yields

$$\sigma(\vec{r}) = \frac{-2\sinh V(\vec{r})}{1+2\cosh V(\vec{r})}. \tag{55}$$

The equation can also be instructively obtained through the Gibbs-Bogoliubov inequality

$$F \le F_{var} \equiv F_0 + \langle H - H_0 \rangle_0, \tag{56}$$

where the index 0 refers to an average with a solvable reference system H_0, taken here as $H_0=-\Sigma_{\vec{r}}B(\vec{r})S(\vec{r})$. Here the local field $B(\vec{r})$ is a variational parameter and the free energy is $F_0=-T\Sigma_{\vec{r}}\log[1+2\cosh\{\beta B(\vec{r})\}]$. The statistical average of $S(\vec{r})$ in the reference system is $\sigma(\vec{r})\equiv\langle S(\vec{r})\rangle_0=2\sinh\beta B/(1+2\cosh\beta B)$ and the average of $H-H_0$ can also be readily performed since the spins are uncorrelated. The optimal local field $B(\vec{r})$, that minimizes F_{var} through $\delta F_{var}/\delta B(\vec{r})=0$ is then directly seen as $B(\vec{r})=-V(\vec{r})$ with the same self-consistency equations as before. Hence $V(\vec{r})$ is indeed the best molecular field to approximate the free energy of the original system.

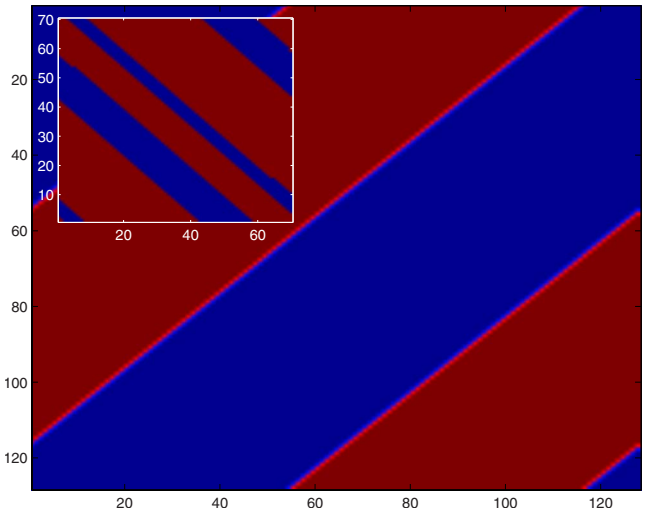

FIG. 2. (Color online) Microstructure obtained from the mean-field analysis of the square-rectangle (SR) spin model. The parameters are $L=128$, $\xi^2=0.5$, $E_0=3$, and $\tau=-2.5$, and stiffness $A_1=4$ with $2A_1/A_3=1$. Twins are oriented along a diagonal as expected. Inset: Twinned ground state from Monte Carlo simulations for the same parameters.

The mean-field equations have been solved iteratively under a cooling ramp in order to study long-lived glassy states.[17] Here we solve the equations for a fixed constant temperature τ starting from an initial random configuration. With an input $\sigma(\vec{r})$ and an fast Fourier transform (FFT) to a Fourier $\sigma(\vec{k})$, it is easy to find $V(\vec{k})$ from the definition, Eq. (51). A reverse FFT to $V(\vec{r})$ is used in Eq. (55) to obtain the next $\sigma(\vec{r})$ and the process repeats. Figure 2 shows twin microstructure obtained by solving the mean-field equations with parameters as in the caption. These twins are similar to those in experiment,[8] to relaxational simulations or to Monte Carlo simulations as in the inset. (Different phases, including certain mazelike textures are also seen in some parameter regimes[17] but do not seem to appear in Monte Carlo simulations.)

Thus a local mean-field approximation to the pseudospin models is useful to study microstructure below ferroelastic transitions. We now (i) study effects of external uniform stress, (ii) make contact with the phase diagram of the Blume-Capel model with uniform OP, and (iii) show how the mean-field equations for $\sigma(\vec{r})$ can be obtained through the least-action principle.

1. Effects of external stress

Twins with oriented, locked-in domain walls of positive energy cost are metastable states, and the uniform single-

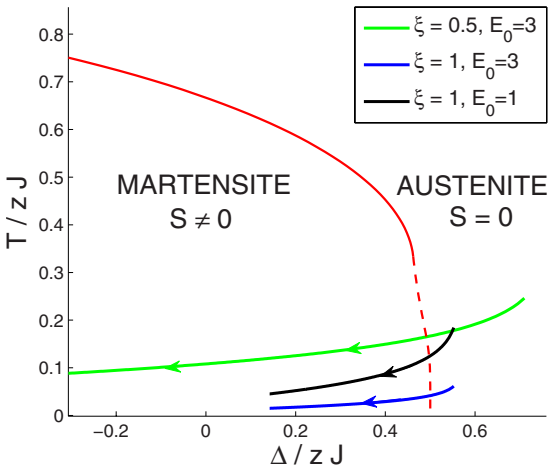

FIG. 3. (Color online) Mean-field phase diagram for the spin-1 model for the SR transition. The red solid line without arrows represents a second-order phase transition and the red dashed line represents a first-order phase transition (Ref. 22), meeting at a tricritical point. The crystal field $\Delta(\tau)$ depends on the temperature τ, so cooling is a phase-diagram trajectory. Three directed trajectories with different sets of parameters are shown, for cooling from $\tau=4/3$ to $\tau=-2.5$.The lines intersect the first-order transition line (dashed) for $\tau \simeq 1$.

variant state without domain walls is the global minimum in free energy. This can be seen by adding an external stress term $h(\vec{r})$ with a simple linear coupling to the mean-field Hamiltonian (49),

$$\beta H_{ext} = -\frac{D_0}{2\bar{\varepsilon}(\tau)} \sum_{\vec{r}} h(\vec{r}) S(\vec{r}). \tag{57}$$

The mean-field self-consistency equations become

$$\sigma(\vec{r}) = \frac{-2\sinh[V(\vec{r}) - (D_0/2\bar{\varepsilon})h(\vec{r})]}{1 + 2\cosh[V(\vec{r}) - (D_0/2\bar{\varepsilon})h(\vec{r})]}. \tag{58}$$

Starting from random texture seeds with a small uniform external stress, $h=0.3$, we obtain a uniform state of $S=\pm 1$ depending on the sign of h: the small stress picks out the global minimum. The twins are self-trapped metastable states that are however quite rigid against stress: for a twinned initial state, a strong stress of about $h=4$ needs to be applied to destroy the twins and to obtain the uniform ground state. Once the twins have vanished, the system fails to return to the original state, i.e., shows hysteretic behavior.

2. Blume-Capel model phase diagram

To make contact with treatments of the Blume-Capel model, we suppress the nonlocal couplings by setting $A_1=0$. The Ginzburg term in Eq. (6) can be recast on a lattice, by setting the gradient to a discrete difference operator $\vec{\nabla} \to \vec{\Delta}$, so that $(\vec{\nabla} S)^2 \to (\vec{\Delta} S)^2 = 4S^2 - 2\Sigma_{\langle \vec{r}\vec{r}' \rangle} S(\vec{r}) S(\vec{r}')$. Then the Hamiltonian is precisely a Blume-Capel model, bilinear in the spins (without the biquadratic term of the Blume-Emery-Griffiths model),[22]

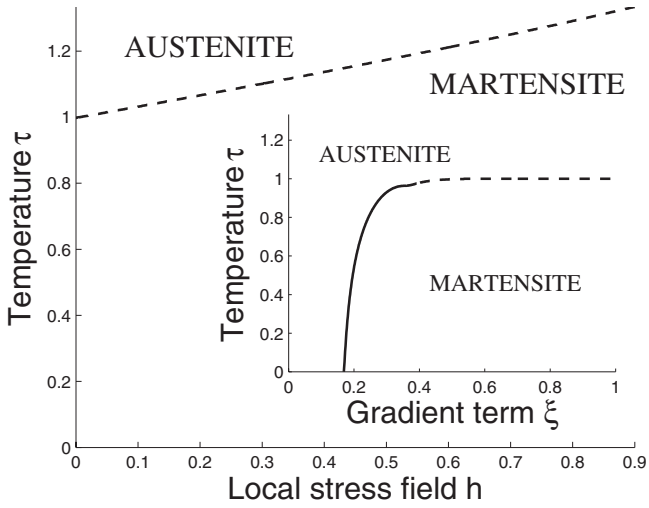

FIG. 4. Mean-field phase diagram of the SR transition in the (h,τ) plane for $\xi=1$. The $h=0$ first-order phase transition temperature of $\tau=1$ moves up with applied stress h. Inset: phase diagram in the (ξ,τ) plane. For ξ large, there is a first-order phase transition line (dashed) with $\tau=1$, while for ξ small, there is a second-order transition line (solid), that moves to lower temperature.

$$H = -J(\tau) \sum_{\langle \vec{r}\vec{r}' \rangle} S(\vec{r}) S(\vec{r}') + \Delta(\tau) \sum_{\vec{r}} S(\vec{r})^2. \tag{59}$$

There is temperature dependence in the on-site crystal-field term $\Delta(\tau) \equiv D_0(\tau)[g_L(\tau) + 4\xi^2]/(2\beta)$ and in the ferromagnetic coupling $J(\tau) \equiv D_0(\tau)\xi^2/\beta$.

The model can be studied within the (uniform) mean-field approximation. An expansion of the mean-field free energy yields an analytical expression for the line of critical points $T_c = zJ/3$; and the location of the tricritical point, $\Delta_c = \frac{2}{3} zJ \log 2$, where $z=4$ is the number of nearest neighbors. Figure 3 shows the well-known phase diagram of this model. Both Δ and J depend on the temperature τ, so although a given temperature corresponds to a point, a cooling path is a line in the phase diagram. These lines intersect the first-order transition curve for $\tau \simeq 1$, the Landau transition temperature between "paramagnetic" austenite and "ferromagnetic" martensite. Figure 4 shows the mean-field phase diagram for two parameter planes (h,τ) and (ξ,τ). In a certain range of parameters, the spin model is consistent with the Landau theory that predicts a first-order phase transition at $\tau=1$.

3. Field theory for $\sigma(\vec{r})$

We show here how the partition function may be transformed to obtain a field theory for $\sigma(\vec{r}) = \langle S(\vec{r}) \rangle$, so the mean-field Eq. (55) results from a saddle-point approximation of a functional integral. Other mean-field equations in this paper can similarly be obtained as saddle-point approximations of field theories.

The partition function can be compactly written as

$$Z = \sum_{\{S\}} \exp\left(\frac{1}{2} \sum_{\vec{r}\vec{r}'} S_{\vec{r}} K_{\vec{r}\vec{r}'} S_{\vec{r}'} \right), \tag{60}$$

where $K_{\vec{r}\vec{r}'} = \beta J(\tau) \delta_{\langle \vec{r},\vec{r}' \rangle} - \frac{D_0 A_1}{2} U(\vec{r} - \vec{r}') - 2\beta\Delta(\tau)\delta_{\vec{r},\vec{r}'}$. The first Kronecker symbol is nonzero only if $\vec{r}$ and $\vec{r}'$ are neighbors.

We note that the kernel $K_{\vec{r}\vec{r}'}$ can be recast using usual matrix notations

$$K_{\vec{r}\vec{r}'} = D_0 \left\langle \vec{r} \left| \xi^2 \nabla^2 - \frac{A_1}{2} U - g_L(\tau) \right| \vec{r}' \right\rangle, \tag{61}$$

where $\langle \vec{r}|U|\vec{r}'\rangle = U(\vec{r}-\vec{r}')$. We may then use the standard Hubbard-Stratonovich transformation $\int e^{-\Sigma_{ij} A_{ij} x_i x_j + \Sigma_i B_i x_i} d^n x = \sqrt{\frac{\pi^n}{\det A}} e^{(1/4) B^T A^{-1} B}$ to find the exact integral representation of the partition function

$$Z = \frac{1}{(2\pi)^{N/2} \sqrt{\det K}} \int \prod_{\vec{r}} d\phi(\vec{r}) e^{-S[\phi]} \tag{62}$$

with the action

$$S[\phi] = \frac{1}{2} \sum_{\vec{r}\vec{r}'} \phi(\vec{r}) K^{-1}_{\vec{r}\vec{r}'} \phi(\vec{r}') - \sum_{\vec{r}} \log\{1 + 2\cosh[\phi(\vec{r})]\}. \tag{63}$$

Finally, we define $\sigma(\vec{r}) = \Sigma_{\vec{r}'} K^{-1}_{\vec{r}\vec{r}'} \phi(\vec{r}')$. The partition function reads

$$Z = \int \mathcal{D}[\sigma(\vec{r})] e^{-S[\sigma]}, \tag{64}$$

where we have defined the formal measure $\mathcal{D}[\sigma(\vec{r})] = \sqrt{\det K}/(2\pi)^{N/2} \Pi_{\vec{r}} d\sigma(\vec{r})$. With this field-theoretical formulation of the partition function, our problem, the mean-field approximation is obtained by minimizing the action

$$S[\sigma] = \frac{1}{2} \sum_{\vec{r}\vec{r}'} \sigma(\vec{r}) K_{\vec{r}\vec{r}'} \sigma(\vec{r}') - \sum_{\vec{r}} \log\left\{ 1 + 2\cosh\left[\sum_{\vec{r}'} K_{\vec{r}\vec{r}'} \sigma(\vec{r}') \right] \right\}. \tag{65}$$

Within the saddle-point approximation, $\sigma(\vec{r}) = \langle S(\vec{r}) \rangle$ so that the field σ is indeed the statistical average of the spin. We note that $V(\vec{r}) = -\Sigma_{\vec{r}'} K_{\vec{r}\vec{r}'} \sigma(\vec{r}')$ [Eq. (52)], so the minimization of the action yields the mean-field Eq. (55), as expected.

B. Triangle/centered-rectangle mean field: $N_{OP}=1$, $N_V=3$

The TCR case spin Hamiltonian is Eq. (38), with spin values $\vec{S} = (0,0), (1,0), (-1/2, \pm\sqrt{3}/2)$ of Eq. (36) and g_L as in Eq. (37). Since $N_{OP}=2$ for the TCR, SO, TO, and CT transitions, their mean-field equations are all formally the same. From the substitution $S_\ell(\vec{r}) = \sigma_\ell(\vec{r}) + \delta\vec{S}(\vec{r})$ and linearization in $\delta\vec{S}(\vec{r}) \equiv S_\ell(\vec{r}) - \sigma_\ell(\vec{r})$ the mean-field Hamiltonian is $\beta H_{MF} \equiv \Sigma_{\vec{r}} \beta h_{MF}(\vec{r}) - C$, as in Eq. (49) but the local contribution is now

$$\sum_{\vec{r}} \beta h_{MF}(\vec{r}) = \sum_{\vec{r}, \ell=2,3} V_\ell(\vec{r}) S_\ell(\vec{r}) = \sum_{\vec{k}, \ell} V_\ell(\vec{k}) S_\ell(\vec{k})^* \tag{66}$$

and $C \equiv \frac{1}{2}\Sigma \langle \beta h_{MF} \rangle = \frac{1}{2} \Sigma_{\vec{k},\ell} V_\ell(\vec{k}) \sigma_\ell(\vec{k})^*$. The functions V_2 and V_3 are defined in Fourier space by

$$V_2(\vec{k}) = P^0_2(\vec{k}) \sigma_2(\vec{k}) + \frac{D_0 A_1}{2} U_{23}(\vec{k}) \sigma_3(\vec{k}), \tag{67}$$

$$V_3(\vec{k}) = P^0_3(\vec{k}) \sigma_3(\vec{k}) + \frac{D_0 A_1}{2} U_{32}(\vec{k}) \sigma_2(\vec{k}), \tag{68}$$

where

$$P^0_\ell(\vec{k}) = D_0 \left[g_L + \xi^2 \vec{k}^2 + \frac{A_1}{2} U_{\ell\ell}(\vec{k}) \right]. \tag{69}$$

Defining P_ℓ in Fourier space as $P_\ell(\vec{k}) \equiv P^0_\ell(\vec{k}) \sigma_\ell(\vec{k})$, the coordinate space mean-field Hamiltonian of Eq. (66) is then

$$\beta h_{MF}(\vec{r}) = \sum_\ell P_\ell(\vec{r}) S_\ell(\vec{r}) + \frac{D_0 A_1}{2} \sum_{\vec{r}'} U_{23}(\vec{r}-\vec{r}') \{ \sigma_2(\vec{r}) S_3(\vec{r}') + \sigma_3(\vec{r}') S_2(\vec{r}) \}. \tag{70}$$

The partition function of this linearized mean-field Hamiltonian can again be factorized as in Eq. (53).

The self-consistency equations as in Eqs. (53) and (54) for the statistical averages $\{\vec{\sigma}(\vec{r})\}$ again have the constant C canceling, so now with $\vec{V} = (V_2, V_3)$ and $\vec{S} = (S_2, S_3)$,

$$\vec{\sigma}(\vec{r}) = \sum_{\vec{S}(\vec{r})} \vec{S}(\vec{r}) e^{-\vec{V}(\vec{r}) \cdot \vec{S}(\vec{r})} / \sum_{\vec{S}(\vec{r})} e^{-\vec{V}(\vec{r}) \cdot \vec{S}(\vec{r})}. \tag{71}$$

In terms of the N_V variant states $\vec{S} = (\cos\phi_m, \sin\phi_m)$ with $m = 1, 2, \ldots, N_V$ this can be formally expressed for TCR, SO, TO, and CT cases as

$$\sigma_2 = \frac{\sum_{m=1}^{N_V} \cos\phi_m e^{-(\cos\phi_m V_2 + \sin\phi_m V_3)}}{1 + \sum_{m=1}^{N_V} e^{-(\cos\phi_m V_2 + \sin\phi_m V_3)}}, \tag{72}$$

$$\sigma_3 = \frac{\sum_{m=1}^{N_V} \sin\phi_m e^{-(\cos\phi_m V_2 + \sin\phi_m V_3)}}{1 + \sum_{m=1}^{N_V} e^{-(\cos\phi_m V_2 + \sin\phi_m V_3)}}. \tag{73}$$

For the TCR case sums over the $N_V=3$ spin values of Eq. (36), this is

$$\sigma_2 = \frac{1}{2} \frac{e^{-(3/2)V_2} - \cosh\left(\frac{\sqrt{3}}{2} V_3\right)}{\left[e^{-V_2} \cosh\left(\frac{V_2}{2}\right) + \cosh\left(\frac{\sqrt{3}}{2} V_3\right) \right]}, \tag{74}$$

$$\sigma_3 = -\frac{\sqrt{3}}{2} \frac{\sinh\left(\frac{\sqrt{3}}{2} V_3\right)}{\left[e^{-V_2} \cosh\left(\frac{V_2}{2}\right) + \cosh\left(\frac{\sqrt{3}}{2} V_3\right) \right]}. \tag{75}$$

where the position dependences of $\sigma_\ell(\vec{r})$ and $V_\ell(\vec{r})$ are left implicit. The coupled Eqs. (74) and (75) were solved iteratively on a $L \times L = 256 \times 256$ lattice with periodic boundary conditions with parameter values $\xi^2 = 0.8$, $A_1 = 5$, $\tau = -6.5$,

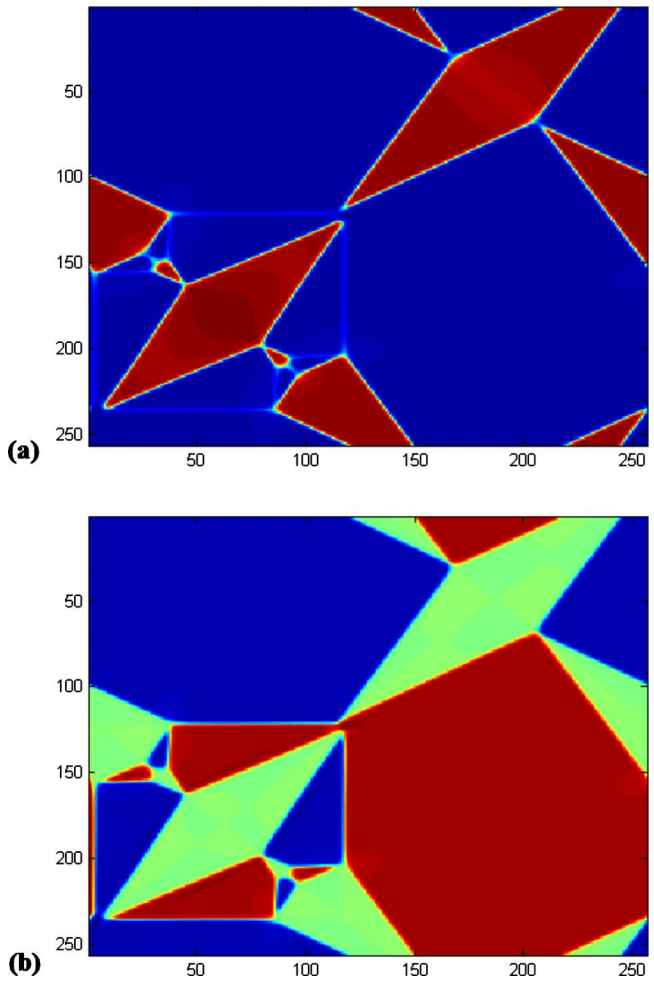

FIG. 5. (Color online) Final-state microstructure obtained from mean-field self-consistency equations for the TCR transition: (a) strain component e_2; (b) strain component e_3. The color code of red (blue) corresponds to positive (negative) values and green to zero. Note the sharp domain walls. Parameters are $L=256$, $\xi^2=0.8$, $E_0=0.01$, scaled temperature $\tau=-6.5$ and stiffness $A_1=5$.

and $E_0=0.01$. Here, and throughout the following other cases, $T_0=1.0$ and $T_c=0.9$.

Figure 5 shows the relaxed microstructure obtained after 10^5 iteration steps. As in continuous-variable simulations in strains or displacements[4,7] we also obtain nested-star patterns as observed in experiments[8] for lead orthovanadate. However, unlike the continuous-variable models which are computationally intensive, the spin models and the local mean-field solutions reach the complex microstructure relatively rapidly.

C. Square/oblique mean field: $N_{OP}=2$, $N_V=4$

The SO case spin Hamiltonian is formally the same as Eq. (38) but with SO case spin values $\vec{S}=(\pm 1/\sqrt{2}, \pm 1/2)$ of Eq. (43), and g_L is as in Eq. (44). Doing a local mean-field approximation as before, the formal self-consistency Eqs. (72) and (73) become

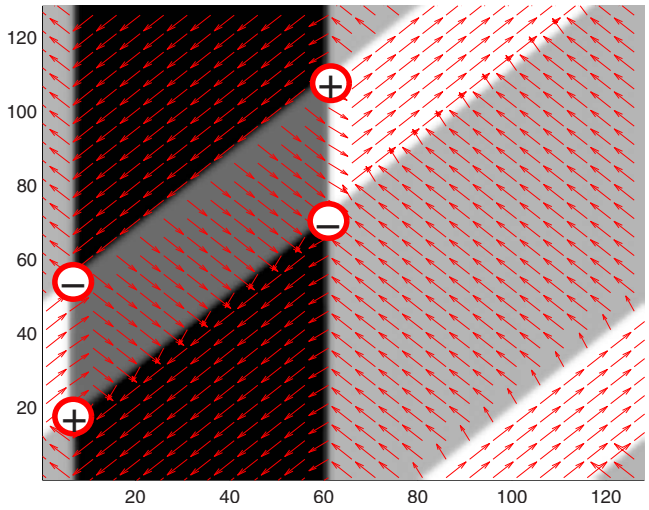

FIG. 6. (Color online) Final-state microstructure from mean-field equations for the SO. The four variants are in four different colors and pseudospin spins orientations are also denoted. The discretized vortices (topological charge +1) and antivortices (topological charge −1), expected in the classical clock models, are also identified. Parameters used are $L=128$, $\xi^2=0.3$, $E_0=0.2$, $\tau=-2.5$, and $A_1=6$.

$$\sigma_2 = -\frac{1}{\sqrt{2}}\frac{2\sinh\left(\frac{V_2+V_3}{\sqrt{2}}\right)+2\sinh\left(\frac{V_2-V_3}{\sqrt{2}}\right)}{\left[1+2\cosh\left(\frac{V_2+V_3}{\sqrt{2}}\right)+2\cosh\left(\frac{V_2-V_3}{\sqrt{2}}\right)\right]}, \tag{76}$$

$$\sigma_3 = -\frac{1}{\sqrt{2}}\frac{2\sinh\left(\frac{V_2+V_3}{\sqrt{2}}\right)-2\sinh\left(\frac{V_2-V_3}{\sqrt{2}}\right)}{\left[1+2\cosh\left(\frac{V_2+V_3}{\sqrt{2}}\right)+2\cosh\left(\frac{V_2-V_3}{\sqrt{2}}\right)\right]}. \tag{77}$$

The coupled equations were solved iteratively on a 128×128 lattice with periodic boundary conditions and for different temperatures τ, starting from an initial random texture. Figure 6 shows that the microstructure obtained for $\tau=-2.5$, has *vortices*, as in the classical clock models or in the XY model. This vortex in the strain field differs of course, from an edge dislocation that is a structural defect in the displacement field. The pseudospin vortex at the meeting point of domain walls is characterized by the winding number or topological charge

$$q_i = \frac{1}{2\pi}\oint_{\Gamma_i} \vec{\nabla}\theta \cdot d\vec{r}, \tag{78}$$

where $\theta(\vec{r})$ is the polar angle of the spin $\vec{S}(\vec{r})$, that equals ϕ_m in the variant regions, and Γ_i is an arbitrary contour surrounding the ith vortex. The topological charge is $q_i=1$ for a vortex and $q_i=-1$ for an antivortex. Thanks to the periodic boundary conditions, we have $\Sigma_i q_i=0$. Vortex solutions for

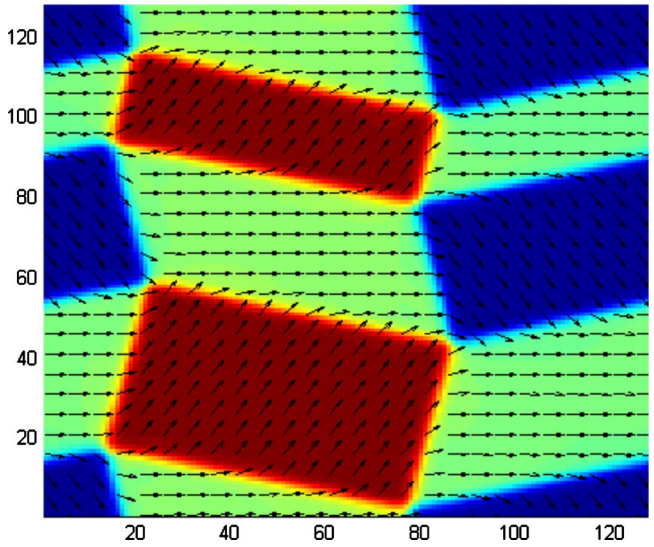

FIG. 7. (Color online) Final-state microstructure from mean-field equations for the TO. The three variants are in three different colors and spin orientations are also shown. Only three of the six variants (see Fig. 8), finally survive. Parameters used are $L=128$, $\xi^2=0.35$, $E_0=0.2$, scaled temperature $\tau=-2.6$, and stiffness $A_1=5$.

complex fields at three-domain meeting points have been considered.[23]

D. Triangle/oblique mean field: $N_{OP}=2$, $N_V=6$

The TO case Hamiltonian is as in Eq. (38) but with TO case spin values $\vec{S}=(0,0),(\pm 1,0),(\pm 1/2,\pm\sqrt{3}/2)$ from Eq. (47), and g_L is as in Eq. (48). The general mean-field self-consistency Eqs. (72) and (73) are then

$$\sigma_2 = -\frac{2\sinh(V_2)+\sinh(I)+\sinh(J)}{1+2\cosh(V_2)+2\cosh(I)+2\cosh(J)}, \quad (79)$$

$$\sigma_3 = -\frac{\sqrt{3}}{2}\frac{2\sinh(I)-2\sinh(J)}{1+2\cosh(V_2)+2\cosh(I)+2\cosh(J)}, \quad (80)$$

where $I=(V_2+\sqrt{3}V_3)/2$ and $J=(V_2-\sqrt{3}V_3)/2$. Figure 7 shows the ground state obtained from these coupled mean-field equations with parameters $L=128$, $\xi^2=0.35$, $E_0=0.2$, $\tau=-2.6$, and $A_1=5$. We note that discrete vortices at the junction of the six martensite variants are seen only during the iterations through transient states as in Fig. 8. The final state microstructure shows no vortices, and only three out of the six variants finally remain, bounded by nonintersecting domain walls, as the other variants vanish during the course of the textural evolution. The suppression of vortices at least for these parameter values could be due to the energy costs of the gradient and power-law terms.

IV. PSEUDOSPIN HAMILTONIAN AND LOCAL MEAN FIELD IN THREE SPATIAL DIMENSIONS

We outline the Hamiltonian derivations for the cubic/tetragonal case and then do a mean-field analysis. The approach can also be followed for other 3D transitions.[17]

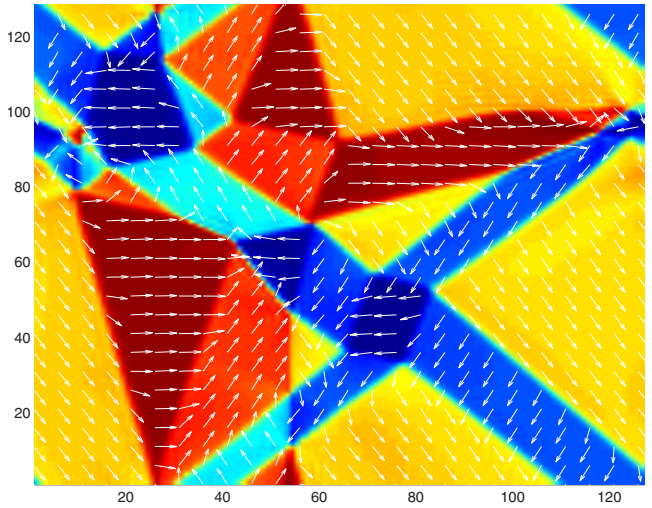

FIG. 8. (Color online) Transient state for the (TO) transition with the six variants with different colors, with parameters as for Fig. 7.

A. Cubic/tetragonal Hamiltonian: $N_{OP}=2$, $N_V=3$

For the cubic-to-tetragonal or "CT" transition, the symmetry-adapted strains are the dilatation $e_1=(1/\sqrt{3})(e_{xx}+e_{yy}+e_{zz})$, the two deviatoric OP strains $e_2=(1/\sqrt{2})(e_{xx}-e_{yy})$, $e_3=(1/\sqrt{6})(e_{xx}+e_{yy}-2e_{zz})$, and the three shear strains $e_4=2e_{yz}$, $e_5=2e_{zx}$, and $e_6=2e_{xy}$.

The OP components are the two deviatoric strains $\vec{e}=(e_3,e_2)$, and the remaining four non-OP compressional and shear strains are e_1,e_4,e_5,e_6. The Landau free-energy invariant under symmetries of the cubic unit cell, was originally given by Barsch and Krumhansl,[10] where the cubic invariant is now $I_3=(e_3^3-3e_3e_2^2)$, and in scaled form is

$$f_L=\tau(e_2^2+e_3^2)-2(e_3^3-3e_3e_2^2)+(e_2^2+e_3^2)^2. \quad (81)$$

The Ginzburg term is formally identical to Eq. (29) but in 3D.

The non-OP terms, harmonic in the four remaining physical strains are

$$f_{non}=\frac{A_1}{2}e_1^2+\frac{A_4}{2}(e_4^2+e_5^2+e_6^2) \quad (82)$$

and are minimized subject to the compatibility constraint (8) in 3D. There are six equations, from cyclic permutations of the labels x,y,z of the two equations

$$2\partial_x\partial_y e_{yz}-\partial_z^2 e_{yy}-\partial_y^2 e_{zz}=0, \quad (83)$$

$$\partial_y\partial_z e_{xx}+\partial_x^2 e_{yz}-\partial_x\partial_y e_{zx}-\partial_x\partial_z e_{xy}=0. \quad (84)$$

By going to Fourier space one finds the second set is an identity, if the first set is satisfied. These constraint equations can be recast in terms of the symmetry-adapted strains $e_1,e_2,\ldots,e_6$. Minimizing $\bar{F}_{non}$ with these constraints (either through Lagrange multipliers[7] or through direct solution for e_4,e_5,e_6 and minimization[17] in the remaining e_1), yields the non-OP strains in terms of the OP strains e_2 and e_3. Substi-

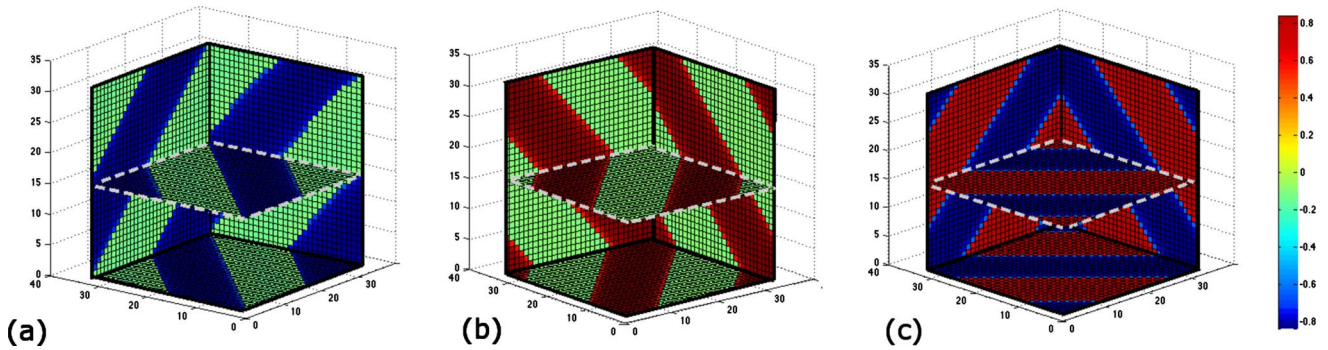

FIG. 9. (Color online) Twins in the (111) plane obtained from the mean-field self-consistency equations for the 3D cubic-to-tetragonal transformation. The color bar represents S_y. The parameters are $L=32$, $\xi^2=10$, $E_0=0.001$, scaled temperature $\tau=-0.5$ and stiffnesses $A_1=4.8$, $A_4=2.4$. The microstructures (a)–(c) show three different twin orientations obtained, for different runs.

tution into the harmonic non-OP free energy yields the compatibility term

$$\bar{F}_{compat} = \frac{1}{2} \sum_{\ell,\ell'=2,3} \sum_{\vec{k}} A_1 U_{\ell\ell'}(\vec{k}) e_\ell(\vec{k}) e_{\ell'}(\vec{k})^*, \qquad (85)$$

where the kernels $U_{\ell,\ell'}(\vec{k})$ in Fourier space[17] are given in the Appendix.

The procedure is formally just as in the TCR case, as the CT case also has the same $N_{OP}=2$, $N_V=3$, pseudospin values $\vec{S}=(0,0),(1,0),(-1/2,\pm\sqrt{3}/2)$ and again $\bar{\varepsilon}(\tau)=3/4(1+\sqrt{1-8\tau/9})$. The spatial dimension only enters in the 3D compatibility potential of kernels, Eq. (85), and in the 3D lattice positions $\vec{r}=(x,y,z)$ and Brillouin-zone wave vectors $\vec{k}=(k_x,k_y,k_z)$.

B. Cubic/tetragonal mean field: $N_{OP}=2$, $N_V=3$

We numerically solved the CT mean-field Eqs. (74) and (75) that are as for the TCR case with the kernels as in the Appendix. We took a $32\times32\times32$ lattice with periodic boundary conditions, and parameters $\xi^2=10$, $E_0=0.001$, $T_0=1$, $T_c=0.9$, and stiffnesses $A_1=4.8$, $A_4=2.4$. Fourier transforms enable a computation at each step of the functions $V_2(\vec{r})$ and $V_3(\vec{r})$. Figure 9 shows the microstructure, with twins at diagonal orientations, as found in continuous-variable simulations.

V. OTHER RELATED MODELS

Modified truncations of these structural-transition free energies can induce other Hamiltonians that can be studied purely as interesting spin models in statistical mechanics.

Let us suppress the zero state, and fix only the circle radius $\varepsilon\to\bar{\varepsilon}(\tau)$, while keeping all continuous polar angles, now denoted by $\theta(\vec{r})$, with values $2\pi>\theta\geq0$,

$$\vec{e}(\vec{r}) = \begin{pmatrix} e_2(\vec{r}) \\ e_3(\vec{r}) \end{pmatrix} \to \bar{\varepsilon}(\tau) \begin{pmatrix} \cos\theta(\vec{r}) \\ \sin\theta(\vec{r}) \end{pmatrix} \qquad (86)$$

so as in the XY model of planar spins, $\vec{S}=(\cos\theta,\sin\theta)$. The Ginzburg discrete-difference term of Eq. (6) then induces an XY-like ferromagnetic interaction. The Landau free energy in polar coordinates in all cases has angular dependence $\bar{f}_L\sim -B\cos N_V\phi$ as in Eqs. (27), (42), and (46). Putting all this together, the free energy induces an XY ferromagnet model with a long-range potential, and a symmetry-breaking local field,

$$\beta H = \frac{D_0}{2}\left\{ -B\sum_{\vec{r}} \cos[N_V\theta(\vec{r})] - 2\xi^2 \sum_{\langle\vec{r},\vec{r}'\rangle} \cos[\theta(\vec{r})-\theta(\vec{r}')] \right\} + \beta H_C[(\theta)]. \qquad (87)$$

Here as $\vec{S}^2=1$, there is no quadratic local term, and $\beta H_C(\{\theta\})$ is a term coupling the continuous-angle variables $\cos\theta(\vec{r})$ and $\sin\theta(\vec{r})$,

$$\beta H_C[\{\theta\}] = \frac{A_1 D_0}{4} \sum_{\vec{r},\vec{r}'} U_{22}\cos\theta(\vec{r})\cos\theta(\vec{r}') + U_{33}\sin\theta(\vec{r})\sin\theta(\vec{r}') + U_{23}\cos\theta(\vec{r})\sin\theta(\vec{r}') + U_{32}\sin\theta(\vec{r})\cos\theta(\vec{r}') \qquad (88)$$

and a partition function

$$Z = \int_{[0,2\pi]^N} \prod_{\vec{r}} d\theta(\vec{r}) \exp(-\beta H[\{\theta(\vec{r})\};\tau]). \qquad (89)$$

This model includes all angles, even away from minima, and so can describe slowly transiting states across N_V saddle points,[23] as in experiment.

Similar XY models with symmetry-breaking fields (without the power-law interaction) have been studied.[24] A dual transform in that case extracts the topological vortices with logarithmic interactions and in this model could also induce a power-law anisotropic vortex interaction. A real-space renormalization-group analysis of the 2D Coulomb gas as in the Kosterlitz-Thouless transition is well known[25] and could be repeated for this model. Renormalization flows in the context of martensitic transitions have been studied in other models.[26]

For strong symmetry breaking in minima angular directions ($|B|$ large), the continuous angle θ become discrete and takes on values that we denote as $\theta\to\phi=\phi_m$, and one gets pure clock models ($\mathbb{Z}_{N_V}$) with a Hamiltonian that now has power-law potentials,

$$\beta H_{clock} = -D_0 \xi^2 \sum_{\langle \vec{r}\vec{r}' \rangle} \cos[\phi(\vec{r}) - \phi(\vec{r}')] + \beta H_C(\{\phi\}). \tag{90}$$

We can even make one more approximation by reducing the XY interaction to a Kronecker-delta coupling, yielding a q-state Potts[19] model with $q=N_V$,

$$\beta H_{Potts} = -D_0 \xi^2 \sum_{\langle \vec{r}\vec{r}' \rangle} \delta_{\vec{S}(\vec{r}),\vec{S}(\vec{r}')} + \beta H_C(\{\phi\}). \tag{91}$$

Potts Hamiltonians with large number of spin components q have been studied as models for configurational glasses.[19]

VI. CONCLUSION

A standard approach to obtaining microstructure of structural transitions is to solve evolution equations for relaxation to a minimum, in continuous variables such as displacements, phase fields or strains.[4–7] We have here considered the reduced Hamiltonian models in *discrete* pseudospins describing four structural transitions in two dimensions, as well as the three-dimensional cubic-to-tetragonal transition. These "clock-zero" models have a zero state as well as clock states, and the pseudospin Hamiltonian has an on-site term, an exchange interaction and a power-law interaction term. For the square/rectangle case, the pseudospin model without power-law interactions corresponds to the Blume-Capel spin-1 model with temperature-dependent couplings. Using a local mean-field approach, we have obtained the microstructure for 2D and 3D transitions, as obtained in continuous-variable strain dynamics. For example, the characteristic nested star microstructure of the triangle transition emerges easily from the mean-field solution.

The textures of the SO and TO transitions, with $N_V=4,6$, which have not been previously studied, include vortex configurations of the $\mathbb{Z}_{N_V+1}$ clock models, at intersections between variant domain walls. The SO final microstructure has positive/negative vortices in regular patterns and all four variants are present. For the TO case, at least for particular parameters, we find the six-variant vortices appear only as transient solutions, with the final state having no vortices, with only nonintersecting closed domains of three variants. Finally, for the three-dimensional cubic/tetragonal transition, we obtain the diagonal twinning that is consistent with previous studies.[4,6,7] In all cases, the local mean-field final microstructure emerges relatively rapidly, compared to the slow evolution toward steady state of the continuum differential-equation dynamics.

Further work can involve studies of pseudospin Hamiltonians[17] for other structural transitions in 2D and 3D in the local mean-field approach. By including quenched disorder, such pseudospin models may be used to study strain glass behavior in martensitic alloys,[21] and relate solutions to the tweed precursors[5] in analogy with spin-glasslike behavior, and to random-field models.[16] Monte Carlo simulations can be used to study martensitic nucleation and growth.[27] Other related spin models of interest in their own right may include geometric nonlinearities that yield complex heirarchical-twin patterns.[2,4] In conclusion, the discrete-variable pseudospin model is an instructive and useful approach to the study of martensitic transformations.

ACKNOWLEDGMENTS

We are grateful to the Center for Nonlinear Science at Los Alamos National Laboratory for summer 2009 student support for RV. We acknowledge useful discussions with Marcel Porta and Avadh Saxena and thank Radha Balakrishnan for help in checking expression 3.41c of Ref. 7(a). This work was carried out under the auspices of the National Nuclear Security Administration of the U.S. Department of Energy at Los Alamos National Laboratory under Contract No. DE-AC52-06NA25396. The National Science and Engineering Research Council (NSERC), Canada, and ICTP, Trieste, are also thanked for support.

APPENDIX: KERNELS FOR THE CUBIC-TO-TETRAGONAL TRANSITION

In this appendix we state the explicit form of the bulk kernels $U_{\ell\ell'}$ obtained elsewhere[17] for the 3D cubic-to-tetragonal transition. To do so we define the coefficients $O_\alpha^{(s)}$ and O_α by

$$O_1^{(4)} = \frac{-1}{\sqrt{3}}(k_y^2 + k_z^2), \quad O_2^{(4)} = \frac{k_z^2}{\sqrt{2}}, \quad O_3^{(4)} = \frac{1}{\sqrt{6}}(2k_y^2 - k_z^2), \tag{A1}$$

$$O_1^{(5)} = \frac{-1}{\sqrt{3}}(k_x^2 + k_z^2), \quad O_2^{(5)} = \frac{-k_z^2}{\sqrt{2}}, \quad O_3^{(5)} = \frac{1}{\sqrt{6}}(2k_x^2 - k_z^2), \tag{A2}$$

$$O_1^{(6)} = \frac{-1}{\sqrt{3}}(k_y^2 + k_x^2), \quad O_2^{(6)} = \frac{1}{\sqrt{2}}(k_x^2 - k_y^2),$$

$$O_3^{(6)} = \frac{-1}{\sqrt{6}}(k_x^2 + k_y^2), \tag{A3}$$

$$O_4 = k_y k_z, \quad O_5 = k_x k_z, \quad O_6 = k_x k_y. \tag{A4}$$

Let $\bar{O}_\alpha^{(s)} = O_\alpha^{(s)}/O_s$ and $G_{\alpha\beta} = \Sigma_s (A_s/A_1)\bar{O}_\alpha^{(s)}\bar{O}_\beta^{(s)}$. The compatibility kernel for the cubic/tetragonal transition can then be written as the 2×2 matrix,

$$U_{\ell,\ell'} = \nu(\vec{k}) \frac{G_{\ell\ell'} + \{G_{\ell\ell'}G_{11} - G_{\ell 1}G_{\ell' 1}\}}{1 + G_{11}}, \tag{A5}$$

where $\nu(\vec{k}) \equiv (1 - \delta_{\vec{k},0})$ sets the non-OP harmonic-energy contribution for uniform strains to its minimum value of zero.

[1] V. K. Wadhawan, *Introduction to Ferroic Materials* (Gordon and Breach, New York, 2000).
[2] K. Bhattacharya, *Microstructure of Martensite* (Oxford University Press, Oxford, 2003); A. G. Khachaturyan, *Theory of structural Transformation in Solids* (Wiley, New York, 1983); J. M. Ball and R. D. James, Philos. Trans. R. Soc. London, Ser. A **338**, 389 (1992).
[3] F. Falk, Z. Phys. B: Condens. Matter **51**, 177 (1983); J.-C. Tolédano and P. Tolédano, *The Landau Theory of Phase Transitions* (World Scientific, Singapore, 1987).
[4] S. H. Curnoe and A. E. Jacobs, Phys. Rev. B **63**, 094110 (2001); A. E. Jacobs, S. H. Curnoe and R. C. Desai, *ibid.* **68**, 224104 (2003); A. E. Jacobs, *ibid.* **52**, 6327 (1995); B. Muite and O. U. Salman, European Symposium on Martensitic Transformations, 2009 (unpublished), p. 03008.
[5] S. Kartha, T. Castan, J. A. Krumhansl, and J. P. Sethna, Phys. Rev. Lett. **67**, 3630 (1991).
[6] Y. H. Wen, Y. Wang, and L. Q. Chen, Philos. Mag. A **80**, 1967 (2000).
[7] T. Lookman, S. R. Shenoy, K. O. Rasmussen, A. Saxena, and A. R. Bishop, Phys. Rev. B **67**, 024114 (2003); K. O. Rasmussen, T. Lookman, A. Saxena, A. R. Bishop, R. C. Albers, and S. R. Shenoy, Phys. Rev. Lett. **87**, 055704 (2001).
[8] C. Manolikas and S. Amelinckx, Phys. Status Solidi A **61**, 179 (1980); J. W. Seo and D. Schryvers, Acta Mater. **46**, 1165 (1998).
[9] J. Dec, Phase Transitions **45**, 35 (1993); A. L. Roytburd, *ibid.* **45**, 1 (1993).
[10] G. R. Barsch, B. Horovitz, and J. A. Krumhansl, Phys. Rev. Lett. **59**, 1251 (1987); B. Horovitz, G. R. Barsch, and J. A. Krumhansl, Phys. Rev. B **43**, 1021 (1991).
[11] S. R. Borg, *Fundamentals of Engineering Elasticity* (World Scientific, Singapore, 1990); E. Kroener, in *Physics of Defects*, Proceedings of the Les Houches Summer School, Session XXV, edited by R. Balian, M. Kleman, and J.-P. Pourier (North Holland, Amsterdam, 1980).
[12] M. Baus and R. Lovett, Phys. Rev. Lett. **65**, 1781 (1990); Phys. Rev. A **44**, 1211 (1991).
[13] R. Ahluwalia, T. Lookman, and A. Saxena, Acta Mater. **54**, 2109 (2006).
[14] M. Porta, T. Castan, P. Lloveras, T. Lookman, A. Saxena, and S. R. Shenoy, Phys. Rev. B **79**, 214117 (2009).
[15] P. A. Lindgård and O. G. Mouritsen, Phys. Rev. Lett. **57**, 2458 (1986); A. M. Bratkovsky, S. C. Marais, V. Heine, and E. K. H. Salje, J. Phys.: Condens. Matter **6**, 3679 (1994); E. Vives, J. Goicoechea, J. Ortin, and A. Planes, Phys. Rev. E **52**, R5 (1995).
[16] B. Cerruti and E. Vives, Phys. Rev. B **77**, 064114 (2008); D. Sherrington, J. Phys.: Condens. Mater. , **20**, 304213 (2008).
[17] T. Lookman, S. R. Shenoy, and A. Saxena, Bull. Am. Phys. Soc. **49**(1), 1315 (2004); S. R. Shenoy and T. Lookman, Phys. Rev. B **78**, 144103 (2008); S. R. Shenoy, T. Lookman, and A. Saxena (unpublished).
[18] G. R. Barsch and J. A. Krumhansl, Phys. Rev. Lett. **53**, 1069 (1984); Metall. Trans. A **19**, 761 (1988).
[19] R. B. Potts, Math. Proc. Cambridge Philos. Soc. **48**, 106–109 (1952); F. Y. Wu, Rev. Mod. Phys. **54**, 235 (1982).
[20] D. M. Hatch, T. Lookman, A. Saxena, and S. R. Shenoy, Phys. Rev. B **68**, 104105 (2003).
[21] S. Sarkar, X. Ren, and K. Otsuka, Phys. Rev. Lett. **95**, 205702 (2005).
[22] M. Blume, Phys. Rev. **141**, 517 (1966); H. W. Capel, Physica (Amsterdam) **32**, 966 (1966); M. Blume, V. J. Emery, and R. B. Griffiths, Phys. Rev. A **4**, 1071 (1971).
[23] H. Buttner, Y. B. Gaididei, A. Saxena, T. Lookman, and A. R. Bishop, J. Phys. A **37**, 8595 (2004); A. Saxena and G. R. Barsch, Physica D **66**, 195 (1993).
[24] J. V. José, L. P. Kadanoff, S. Kirkpatrick, and D. R. Nelson, Phys. Rev. B **16**, 1217 (1977).
[25] J. M. Kosterlitz and D. J. Thouless, J. Phys. C **6**, 1181 (1973).
[26] M. Rao, S. Sengupta, and H. K. Sahu, Phys. Rev. Lett. **75**, 2164 (1995); K. M. Crosby and R. M. Bradley, Philos. Mag. Lett. **75**, 131 (1997).
[27] N. Shankaraiah, K. P. N. Murthy, T. Lookman, and S. R. Shenoy (unpublished).